Published in final edited form as:
J Comp Neurol. 2011 December 15; 519(18): 3802–3814. doi:10.1002/cne.22734.

Quantitative Analysis of Glutamatergic Innervation of the Mouse Dorsal Raphe Nucleus Using Array Tomography

Mariano Soiza-Reilly[1,2,*] and **Kathryn G. Commons**[1,2]

[1]Department of Anesthesiology, Perioperative, and Pain Medicine, Children's Hospital Boston, Boston, Massachusetts 02115

[2]Department of Anaesthesia, Harvard Medical School, Boston, Massachusetts 02115

Abstract

Serotonin (5-hydroxytryptamine, 5-HT) containing neurons located in the dorsal raphe nucleus (DR) comprise the main source of forebrain 5-HT and regulate emotional states in normal and pathological conditions including affective disorders. However, there are many features of the local circuit architecture within the DR that remain poorly understood. DR neurons receive glutamatergic innervation from different brain areas that selectively express three different types of the vesicular glutamate transporter (VGLUT). In this study we used a new high-resolution imaging technique, array tomography, to quantitatively analyze the glutamatergic innervation of the mouse DR. In the same volumetric images, we studied the distribution of five antigens: VGLUT1, VGLUT2, VGLUT3, the postsynaptic protein PSD-95, and a marker for 5-HT cells, the enzyme tryptophan hydroxylase (TPOH). We found that all three populations of glutamatergic boutons are present in the DR; however, the density of paired association between VGLUT2 boutons and PSD-95 was ≈2-fold higher than that of either VGLUT1- or VGLUT3-PSD-95 pairs. In addition, VGLUT2-PSD-95 pairs were more commonly found associated with 5-HT cells than the other VGLUT types. These data support a prominent contribution of glutamate axons expressing VGLUT2 to the excitatory drive of DR neurons. The current study also emphasizes the use of array tomography as a quantitative approach to understand the fine molecular architecture of microcircuits in a well-preserved neuroanatomical context.

INDEXING TERMS

glutamate axons; VGLUT1; VGLUT2; VGLUT3; PSD-95; serotonin

The dorsal raphe nucleus (DR) represents the main source of forebrain serotonin (5-hydroxytryptamine, 5-HT) (Steinbusch et al., 1981; Molliver, 1987) and plays a crucial role in controlling emotional states, REM sleep, and appetitive and aggressive behavior (Jacobs and Azmitia, 1992; Takahashi et al., 2010). Additionally, DR dysfunction has been implicated in the pathophysiology of affective disorders including anxiety and depression (Stockmeier et al., 1997; Arango et al., 2002). The primary excitatory drive of 5-HT neurons located in the DR arises from glutamate neurons in cortical and subcortical regions including several hypothalamic nuclei (Kalén et al., 1985; Lee et al., 2003). Thus, the normal functioning of the DR relies on appropriate activity of these glutamatergic inputs onto 5-HT neurons, and dysregulation of glutamate neurotransmission within the DR has been implicated in depression (Paul and Skolnick, 2003).

*CORRESPONDENCE TO: Mariano Soiza-Reilly, PhD, Children's Hospital Boston, 300 Longwood Ave., Boston, MA 02115. mariano.soiza-reilly@childrens.harvard.edu.

Different populations of glutamate-containing axons can be distinguished by the presence of specific types of the vesicular glutamate transporter (VGLUT1, VGLUT2, and VGLUT3). Each of these VGLUTs has the capacity to transport the neurotransmitter glutamate into synaptic vesicles (Bellocchio et al., 2000). In the adult, there is a topographically segregated expression pattern of each VGLUT type. That is, VGLUT1 is highly expressed in cortical structures including hippocampus and cerebellum, whereas VGLUT2 is widely expressed in subcortical areas with minor expression in cortical neurons (Fremeau et al., 2001; Herzog et al., 2001; Kaneko and Fujiyama, 2002; Kaneko et al., 2002; Varoqui et al., 2002). VGLUT3 has an unusual distribution and is found in specific subsets of cells that coexpress other neurotransmitters including hippocampal interneurons, cholinergic striatal interneurons, and serotonin cells from the dorsal and median raphe nuclei (Schafer et al., 2002; Fremeau et al., 2002; Gras et al., 2002; Hioki et al., 2004; Herzog et al., 2004; Shutoh et al., 2008; Fu et al., 2010). In addition, VGLUT3 is found in a group of non-5-HT neurons locally within the DR (Commons, 2009; Hioki et al., 2010). Therefore, different populations of glutamate axons innervating the DR can be distinguished by the specific types of VGLUT present at their axonal boutons, and correlates with the relative contributions of glutamate excitatory inputs arising from different brain areas to DR circuits.

Quantification of axon terminals using conventional immunohistochemistry is impacted by the differential penetration of antibodies into thick sections. A new highresolution imaging technique called array tomography allows for the quantitative analysis of synaptic architecture (Micheva and Smith, 2007, Micheva et al., 2010a). This technique involves the immunostaining and imaging of arrays of ultrathin (70 nm) serial sections using conventional fluorescence microscopy. Subsequently, images are aligned and 3D volumetric images rendered, allowing for a more precise mapping of antigen distribution. This both allows for increased resolution, primarily due to increased resolution in the z-axis, and eliminates issues related to antibody penetration because antigens are available on the section surface (Koffie et al., 2009; Datwani et al., 2009; Micheva et al., 2010a). The immobilization and strength of the sections embedded in plastic leads to another important advantage, that is, the ability to strip immunofluorescence and re-immunolabel, resulting in visualizing multiple antigens with respect to each other. In this study we used array tomography to quantitatively analyze the distribution of glutamate axonal boutons containing all three different types of VGLUT and their associations with postsynaptic markers for glutamatergic synapses (PSD-95) as well as with 5-HT neurons in the mouse DR.

MATERIALS AND METHODS

Tissue preparation

All procedures related to the care and treatment of animals were approved by the Institutional Animal Care and Use Committee at Children's Hospital Boston and conformed to National Institutes of Health guidelines. All efforts were made to minimize the number of mice necessary to produce reliable scientific data and experiments were designed to reduce any distress experienced. Three adult C57BL/6 mice were anesthetized with sodium pentobarbital (80–120 mg/kg) and transcardially perfused through the ascending aorta with 50 ml of 4% paraformaldehyde in 0.1 M phosphate buffer (pH 7.4). Brains were removed and postfixed in 4% paraformaldehyde overnight at 4°C and then equilibrated in 25% sucrose in phosphate-buffered saline (PBS) for 24 hours. Thereafter, 100-μm thick sections through the midbrain were cut using a Vibratome (PELCO 102; Ted Pella, Redding, CA). Sections including the middle part of the DR (Fig. 1) (anteroposterior −4.36 to −4.72 mm from the bregma according to Paxinos and Franklin [2001]) were processed for array tomography (Micheva and Smith, 2007; Micheva et al., 2010b).

To prepare sections for array tomography, thick tissue sections were dehydrated in graded series of alcohol up to 70% ethanol (5 minutes each step at room temperature). Subsequently, the tissue was infiltrated in a 1:3 mixture of 70% ethanol and LRWhite resin (medium grade, SPI Supplies) for 5 minutes, then three times of 5 minutes each in 100% LRWhite. After that the tissue was infiltrated in LRWhite overnight at 4°C. On the next day sections were flat-embedded between a glass slide (to provide a flat surface) and a sheet of ACLAR plastic (Ted Pella) to facilitate removal of the tissue section, and polymerized 24 hours at 55°C. Subregions of the DR representing midline areas where 5-HT neurons are densest were selected using light- and darkfield microscopy. These areas were excised from the tissue section and mounted on EMBed 812 chucks using superglue. With the aid of a dissecting microscope, the area including the DR was further trimmed using a razor blade to a trapezoidal shape (≈2.5 × 1.5 mm). Each block contained both studied subregions of the DR (Fig. 1).

LRWhite sections

Adhesive cement (Weldwood Contact Cement) diluted in xylene was applied with a paintbrush to the top and bottom of the block face to facilitate collection of serial sections (Micheva et al., 2010b). After the glue had dried, series of 25 or more sections 70-nm thick were cut in ribbons using Jumbo Histo Diamond Knife (Diatome, Fort Washington, PA) and an ultramicrotome (Leica Ultracut, Deerfield, IL). The ribbons were mounted on glass coverslips. Coverslips were previously subbed (coated with 0.1% gelatin and 0.01% chromium potassium sulfate) to facilitate adherence of the sections through multiple rounds of immunostaining. Coverslips containing ribbons were placed on a hot plate (60°C) for 30 minutes, then stored at room temperature until processing for immunofluorescence.

Immunofluorescence labeling

Primary antisera raised against the tryptophan hydroxylase (TPOH; sheep, 1:200; Millipore, Bedford, MA), VGLUT1, VGLUT2, and VGLUT3 (all three guinea pig, 1:1,000; Millipore), and synapsin I (rabbit, 1:100; Millipore) were used, while PSD-95 was detected by using a monoclonal antibody (rabbit, 1:200; Cell Signaling Technologies, Beverly, MA) (Table 1). For quantitative analysis three antibodies from different hosts were applied together (e.g., PSD-95, VGLUT1, and TPOH) and imaged, followed by an antibody elution. To control for possible antigenicity changes after several staining/elution rounds, we included in each round immunolabeling for TPOH and PSD-95 jointly with only one type of VGLUT randomly assigned. Sections were then re-stained with a different set of antibodies and re-imaged. This resulted in volumetric images containing immunolabeling for all three VGLUTs, PSD-95, and TPOH after three rounds of immunolabeling. An additional subset of sections was immunolabeled with synapsin I to evaluate the colocalization with each type of VGLUT.

For immunolabeling the sections were encircled with a PAP pen (Aqua-Hold, Scientific Device Laboratory) and preincubated first with 50 mM glycine in Tris saline buffer (TSB; pH 7.6) and then with a blocking solution (0.05% Tween; 0.1 bovine serum albumin [BSA] in TSB) for 5 minutes each. Subsequently, primary antisera were diluted together in blocking solution and were incubated with the sections for 2 hours. Following incubation, sections were intensely rinsed with TSB three times by subjecting them to a continuous flow of buffer for ≈20 seconds using a plastic transfer pipette. This was followed by incubation in the same buffer in a humid chamber for 10 minutes. Fluorescent conjugated secondary antisera raised in donkey with minimal crossreactivity to other species were used (Alexa 488 and 647, 1:150; Invitrogen, Carlsbad, CA; CY3, 1:300; Jackson ImmunoResearch, West Grove, PA). Secondary antisera were centrifuged at 13,000 rpm for 3 minutes before use. Sections were incubated with the secondary for 15 minutes and rinsed as previously

described. The coverslips with sections were then mounted on a glass slide using a glycerol based mounting media (90% glycerol in PBS, pH 9.0) and imaged.

To elute the applied antibodies, the mounting medium was washed away with distilled H_2O and coverslips were incubated with a solution containing 0.02% sodium dodecyl sulfate (SDS) and 0.2 M NaOH in distilled H_2O for 20 minutes. After two washes with TSB and one with distilled H_2O, 10 minutes each, coverslips were dried and placed on a hot plate (60°C) for 30 minutes (Micheva et al., 2010b). Upon re-immunolabeling, negative controls where the primary antisera were omitted were run to corroborate the complete elution of primary antibodies.

As a positive control for reproducibility of immunolabeling we also performed a quantitative analysis of PSD-95 puncta, either associated or not with 5-HT cells, in the same stack of images after several rounds of staining/elution (Fig. 2).

Antibody characterization

The list of primary antibodies used in this study is provided in Table 1. The guinea pig anti-VGLUT1 polyclonal antisera and guinea pig anti-VGLUT2 have been similarly characterized. Western blot of rat tissue using these anti-sera yield single bands at the expected sizes of 60 kDa for VGLUT1 (Melone et al., 2005) and 52 kDa for VGLUT2 (as reported by the manufacturer). Also reported by the manufacturer, preabsorption with the immunogen peptide abolishes immunolabeling for both antisera. In addition, immunolabeling for electron microscopy in the DR using each of these antisera individually results in labeling of axon terminals (Commons et al., 2005). Finally, other array tomography studies have shown correlation between immunolabeling with both of these antisera individually and synapsin I in the mouse cortex, consistent with the identification of axonal boutons (Micheva et al., 2010a).

According to manufacturer's specification, the guinea pig anti-VGLUT3 polyclonal antisera recognize a single band of ≈65 kDa on western blots from lysate of rat-derived PC12 cells. Preabsorption with the immunogen peptide eliminates immunostaining on rat brain tissue, as reported by the manufacturer as well as in the literature (Gabellec et al., 2007; Shutoh et al., 2008). Using conventional immunofluorescence techniques, the pattern of immunolabeling using these antisera coincides with the described distribution of immunoreactivity obtained with other VGLUT3 antisera in the DR and other areas including the hippocampus, confirmed by both us (Commons and Serock, 2009) and others (Gabellec et al., 2007). Furthermore, the resulting immunolabeling is consistent with the known distribution of cells expressing VGLUT3 mRNA (Fremeau et al., 2002; Gras et al., 2002; Commons, 2009; Hioki et al., 2010).

The sheep anti-TPOH polyclonal antiserum is affinity-purified and produces a major band of 55 kDa on western blots from rat dorsal raphe that corresponds to the predicted size of TPOH, as reported by the manufacturer. Immunofluorescence labeling with this antibody produces a pattern of labeling consistent with the well-known distribution of 5-HT neurons (Steinbusch, 1984). Although this antiserum has a high sensitivity for TPOH, it also has some crossreactivity to tyrosine hydroxylase that can be detected using western blots from rat dorsal raphe (manufacturer description) or immunohistochemistry. Within the DR, there are dopaminergic neurons that may be detected using this antiserum, but they are most abundant rostral to the areas selected for analysis.

As reported by the manufacturer, the rabbit anti-PSD-95 monoclonal antibody recognizes a single band of 95 kDa on western blots from extracts of rat brain and human cerebellum, consistent with the expected size of PSD-95. To characterize this antibody we performed

double immunolabeling with this antiserum and a well-characterized mouse monoclonal antibody (Neuromab cat. no. 75-028; Micheva et al., 2010a) on tissue sections processed for array tomography, and observed a very high level of colocalization (data not shown).

The rabbit anti-synapsin I polyclonal antiserum recognizes two bands of 77 and 80 kDa on western blots of mouse brain extracts, corresponding to the expected size of synapsin Ia and Ib, respectively. The immunolabeling produced with this antiserum is blocked by preadsorption of antibody with synapsin I according to the manufacturer's description. Previous studies using array tomography have shown a dense punctate distribution of immunolabeling when using this antibody that has a high correlation with several other markers of synaptic vesicles (Micheva et al., 2010a). Moreover, examination of array tomography sections by electron microscopy as well as by using postembedding immunogold labeling have shown a selective localization in axon terminals in mouse cortex (Micheva et al., 2010a).

Microscopy and image processing

Sections were imaged on an Olympus fluorescence microscope using an Olympus 60× NA 1.42 Plan Apochromat oil objective and a Hamamatsu Orca ER camera and Slidebook software (3i). Dorsal and ventral midline areas of the mid DR were imaged. Images from serial sections were converted into stacks and aligned using the ImageJ-based Fiji software and the StackReg plug-in (Thevenaz et al., 1998). The TPOH immunolabeling was used to align serial images in final volumetric images using both rigid and affine registration processing.

The enhance contrast and subtract background functions of Fiji were also used on images before the analysis. Specifically, the image's contrast was defined at 0.1% of saturated pixels, while the spurious background was removed using a rolling ball radius of 20 pixels for VGLUTs and PSD-95, and 50 pixels for TPOH immunolabeling.

Volumetric images were rendered using the 3D view function of Fiji, using a resampling factor of 1. Only for visualization purposes, saturation histograms of both single-section and volumetric images were also adjusted using Adobe Photoshop (San Jose, CA).

Quantitative analysis

A total of 12 stacks containing at least 25 images each were imaged. This consisted of two stacks per block (one for each region of interest), two blocks per mouse with three mice analyzed. For each stack, the quantitative analysis involved sampling an area of 90 × 90 μm arbitrarily selected within each anatomical region of interest of dorsal and ventral midline DR. Image stacks were converted to binary images using the threshold function for each channel. The threshold level was initially selected using the JACoP plug-in (Bolte and Cordelières, 2006) and in some cases manually adjusted such that immunolabeled objects were selectively included with minimal background. Subsequently, total particles per volume were counted using the Object Counter 3D plug-in. Puncta appositions (e.g., PSD-95/VGLUT1) and associations with TPOH-positive areas were identified using the multiply operation of the image calculator function. After that, identified objects were counted using the Object Counter 3D plug-in and expressed as number of puncta per μm^3 of brain tissue. Results from each stack and region were averaged to generate a region mean per individual mouse, and subsequently results per mouse were averaged together.

Due to the abundance of many synaptic markers, overlapping spatial distributions might occur by chance. Thus, spatial relationships between PSD-95 and VGLUTs puncta were further examined by a cross-correlation analysis of pixels using the method described by van Steensel et al. (1996) and the JACoP plug-in (Bolte and Cordelières, 2006). Cross-

correlation values were computed over a range of lateral displacement distances in μm, using binary images of both channels analyzed.

Statistical analysis

The individual data of all three mice were analyzed using a two-way analysis of variance (ANOVA) with VGLUT types and subregion as between-subjects factors. Significant interactions between factors were analyzed by simple effects ANOVA and post-hoc comparisons were done using the Scheffe test. The level of significance was established at $P < 0.05$.

RESULTS

Sampling and methodological controls

We focused our analysis on ventral (v) and dorsal (d) midline subregions of the mid DR (Fig. 1) because they contain the highest density of 5-HT neurons (Steinbusch, 1984; VanderHorst and Ulfhake, 2006). Array tomography allows examination of a broader XY area in comparison to electron microscopy; therefore, in this study both areas of the DR quantified were contained in the same block and sections. The density of TPOH labeled structures was comparable in these two areas and accounted for about 14% of the total volume. Examination of tissue sections processed for immunolabeling without primary antisera or for elution of immunolabeling revealed negligible fluorescence labeling.

In order to control for possible changes in antigenicity due to several rounds of staining/elution, we included immunolabeling for TPOH and PSD-95 in each round. Analysis of the reproducibility of immunolabeling with these antigens between different rounds of staining/elution showed a very similar pattern of immunolabeling for PSD-95 and TPOH, indicating that the antigenicity is substantially preserved at least after three rounds (Fig. 2A-C). That is, a high proportion of the same pixels were relabeled after consecutive rounds of staining/elution for TPOH ($r = 0.94$) and PSD-95 ($r = 0.89$) (Fig. 2D,E). Remaining pixels that were not repeatedly detected either represent nonspecific immunolabeling or specific immunolabeling that falls below the level of detection in two of three rounds. In addition, the total amount of PSD-95-immunolabeled puncta either associated or not with TPOH-immunolabeled processes was also similar for the same stack of images among different rounds of staining/elution (Fig. 2F).

Volumetric images rendered from images of serial sections illustrate the high-resolution achieved in array tomography (Fig. 3). Therefore, individual synaptic elements (e.g., PSD-95) and their associations with TPOH-immunolabeled processes can be easily detected and subjected to quantitative automated analysis.

Glutamatergic axon terminals within the DR

Qualitative examination of the patterns of immunolabeling revealed that immunolabeling for all three types of VGLUT yielded punctate labeling widespread in both subregions of the DR studied (Fig. 4A,B), consistent with a primary localization within axons. In general, puncta immunolabeled for one type of VGLUT did not contain labeling for either of the other two. Also, immunolabeling for each VGLUT often appeared at the same location through several serial sections (Fig. 5), although there were instances where labeling appeared only in single sections.

We completed two different types of analyses to quantify the distribution of VGLUT immunolabeling. The first one involved a broad and less conservative approach of quantifying all individual immunolabeled elements within volumetric images in total and in

association with TPOH immunolabeling. The second approach was a more conservative analysis where a contingency was imposed to exclude biologically less relevant and nonspecific immunolabeling. In a subset of the data we analyzed VGLUT-immunolabeled puncta that colocalized with synapsin I. Subsequently, we did a comprehensive analysis of VGLUT-positive elements that had a relationship to the postsynaptic protein PSD-95. We focused on the PSD-95 analysis with the aim of getting specific insight into instances of VGLUT immunolabeling that corresponded to potential synapses.

The first analysis of all instances of VGLUT immunolabeling showed a similar regional distribution of each type of VGLUT in both the dorsal and ventral portions of the midline DR, as there were no significant interaction between subregion and VGLUT type ($F_{2,12}$ = 0.75, P = 0.492) or a main effect of subregion ($F_{1,12}$ = 1.37, P = 0.264) (Fig. 5E,F). However, we found differences in the density of each VGLUT type within both studied subregions ($F_{2,12}$ = 11.38, P < 0.002). Specifically, we found that there was a greater density of VGLUT2-immunolabeled puncta than VGLUT1 puncta overall in the DR (P < 0.002), and nonsignificantly different from VGLUT3 (P = 0.06) (Fig. 5E,F).

In order to get a measure of the potential interactions between puncta immunolabeled for each of VGLUTs and 5-HT cells, we quantified instances where VGLUT-immunolabeled objects overlapped with TPOH-labeled profiles. This accounted for 42% of the total number of VGLUT1-3-immunolabeled puncta in the ventral DR and 35% in the dorsal DR. We did not find a significant interaction effect between subregion and VGLUT type ($F_{2,12}$ = 0.10, P = 0.904) or a selective association with one type of VGLUT versus another ($F_{2,12}$ = 2.45, P = 0.128). Also, the total amount of VGLUT1-3 puncta associated with 5-HT neurons was not significantly different between both subregions ($F_{1,12}$ = 0.95, P = 0.350) (Fig. 5E,F).

Colocalization of VGLUTs with synapsin I

This first analysis of total VGLUT-immunolabeled puncta is likely an overestimation of axon terminals because both smaller objects and potentially nonspecific labeling may be included. We further examined whether these VGLUT-positive puncta might also be related to a general marker for presynaptic axon terminals such as synapsin. Although this protein is thought to be one of the best general markers for synaptic boutons, it may be present at different levels in different populations of axon terminals and/or at low levels. Therefore, colocalization with synapsin would provide a conservative estimate of synaptic boutons (Micheva et al., 2010a). For this analysis we processed two of the volumes sampled containing 29 sections including both dorsal and ventral subregions of the DR. We found that 26%, 34%, and 30% of VGLUT1-, VGLUT2-, and VGLUT3-immunolabeled objects, respectively, were dually labeled for synapsin, confirming that at least this subset of VGLUT-labeled puncta correspond to accumulations of synaptic vesicles. Remaining puncta could be accounted for among various possible groups including synaptic boutons with subthreshold levels of synapsin, a biologically relevant accumulation of VGLUT protein that is not associated with significant synapsin, and/or non-specific immunolabeling.

Apposition of glutamate axon boutons and PSD-95

In order to specifically study synaptic associations, we subsequently analyzed the density of VGLUT1-3-immunolabeled puncta in close apposition with the postsynaptic protein PSD-95 (Fig. 6). First, we found that PSD-95 independently was highly abundant and equally distributed in both studied subregions of the DR ($F_{1,12}$ = 0.24, P = 0.636) (Figs. 4, 5A). PSD-95 puncta could be detected through several consecutive sections (Fig. 4C), and was visible on the perimeter of TPOH-labeled processes and cell bodies. In addition, it was noted that some PSD-95 puncta were not on the surface of TPOH dendrites, but rather appeared within what is likely the cytoplasmic compartment of TPOH-immunolabeled profiles,

possibly corresponding to components of the postsynaptic densities in transit to or from synaptic sites. A large population (≈65%) of PSD-95 puncta was not associated with any of the VGLUT presynaptic partners. In addition, in both studied subregions a substantial proportion (≈70%) of PSD-95 was not associated with 5-HT neurons, indicating likely association with non-5-HT cell processes (Fig. 5A).

Only a fraction of the total number VGLUT-immunolabeled elements was found in close apposition to PSD-95. 29% of VGLUT2 puncta were associated with PSD-95 while lower percentages, 20%, and 14% of VGLUT1 and VGLUT3 puncta, respectively, were associated with PSD-95. The higher rate of association of VGLUT2 with PSD-95, coupled with the overall abundance of VGLUT2 puncta, resulted in a higher absolute density of VGLUT2/PSD-95 pairs than VGLUT1/PSD-95 or VGLUT3/PSD-95 pairs (Fig. 6A,B) ($F_{2,12} = 57.03$, $P < 10^{-4}$). Depending on the subregion and VGLUT type, VGLUT2/PSD-95 pairs predominated by 1.8–2.5-fold. Consistent with the higher density of VGLUT2/PSD-95 pairs, cross-correlation analysis between PSD-95 and VGLUT-immunolabeled pixels showed a higher degree of colocalization for VGLUT2 puncta with PSD-95 in comparison to VGLUT1 or VGLUT3 (Fig. 6F). We also performed, as a control, cross-correlation analysis between VGLUT1 and VGLUT2 puncta, and found no evidence for a relationship (Fig. 6F). Thus, all three VGLUTs specifically associate with PSD-95, and VGLUT2 predominates in this relationship.

We then evaluated the triple association between VGLUT/PSD-95 and 5-HT cells (Fig. 6). Only a proportion of the total number of VGLUT/PSD-95 pairs were associated with TPOH-immunolabeled profiles: 28%, 23%, and 32% for VGLUT1, 2, and 3, respectively. Thus, VGLUT2/PSD-95 pairs were somewhat underrepresented in the relationship to TPOH, and lost their consistent 2-fold predominance over VGLUT1 and VGLUT3. However, there were still significant differences in abundance of appositions containing each type of VGLUT in the vDR ($F_{2,6} = 9.31$, $P < 0.01$) and the dDR ($F_{2,6} = 12.21$, $P < 0.01$). In the vDR, VGLUT2/PSD-95 pairs in association with TPOH were 33% more numerous than those containing VGLUT3 ($P < 0.02$) and 25% more than those containing VGLUT1, although in this case statistical significance was not reached ($P = 0.06$) (Fig. 6A,B). In the dDR, the number of VGLUT2-containing appositions associated to 5-HT cells were 2-fold more numerous than those containing VGLUT1 ($P < 0.01$) and 22% more than VGLUT3 ($P < 0.05$).

To summarize the differences in the synaptic arrangements in vDR versus dDR, there was a greater density overall of VGLUT/PSD-95 pairs in the vDR in comparison to dDR ($F_{1,12} = 12.79$, $P < 0.004$). In addition, VGLUT1-PSD-95 pairs were more commonly associated with TPOH cells in the vDR in comparison to the dDR ($F_{1,4} = 39.30$, $P < 0.003$).

DISCUSSION

In this study we used array tomography to quantitatively analyze the density of different populations of glutamate axonal boutons within the DR, identified by the presence of three different types of VGLUT, and their association with a postsynaptic marker for glutamatergic synapses, PSD-95. While puncta immunolabeled for all three VGLUTs were present in the DR and associate with PSD-95, VGLUT2 was the most abundant, suggesting it provides the primary source of synaptic drive in the DR. However, the frequencies of synaptic associations of each of the VGLUT-type with TPOH-labeled process differed from their overall association with PSD-95, consistent with the possibility that 5-HT and non-5-HT cells could receive different complements of glutamatergic innervation. Furthermore, regional differences between dorsal and ventral components of the DR were detected. Taken

together, our results indicate array tomography provides a sensitive technique to evaluate features of synaptic connectivity.

Methodological considerations

Evaluation and interpretation of immunolabeling using array tomography presents new challenges. In conventional immunofluorescence there are large 3D volumes where labeling can be evaluated in a larger context. When using electron microscopy, immunolabeling is evaluated in the context of subcellular structure. In array tomography objects are sectioned such that context is less readily apparent and only afforded by the presence of immunolabeling for other antigens. In this study we performed two different quantitative analyses to study glutamatergic axons into the DR. The first approach was an inclusive one where we calculated the total density of puncta immunolabeled for each of the three types of VGLUTs. This analysis is vulnerable to false-positive error due to the potential inclusion of spurious immunolabeling. In the second analysis a contingency was imposed such that immunolabeling for each VGLUT was analyzed with respect to a second marker, primarily PSD-95. This analysis could be overly conservative because of the likelihood of instances where PSD-95 is present but at levels below the limits of sensitivity of the technique, or PSD-95 is absent, but VGLUT immunolabeling nevertheless represents a valid and biologically relevant situation. However, there were many more statistically significant findings in the more stringent analysis using the contingency of association between VGLUT and PSD-95. This suggests that imposing contingencies can substantively reduce technical noise, increasing the sensitivity of the technique. Given that array tomography is also amenable to multiple rounds of immunolabeling, the strength of the approach may lie in understanding relationships between multiple antigens.

We found a dense and reproducible distribution of PSD-95 in the DR, not always related to a VGLUT presynaptic partner. PSD-95 represents the most abundant protein in the postsynaptic densities at glutamatergic synapses (Peng et al., 2004; Cheng et al., 2006), and plays a complex role in regulating synapse formation and function by interacting intracellularly with a large number of proteins (Han and Kim, 2008; Keith and El-Husseini, 2008). Recently, PSD-95 has also been implicated in the intracellular distribution and function of 5-HT2A and 5-HT2C receptors (Abbas et al., 2009), both functional in the DR (Freitas et al., 2008). Thus, PSD-95 that is not in association with a VGLUT may represent synaptic components in transit to or from functional sites, or may be associated with nonglutamatergic axons that form symmetric synapses.

In our analyses of all VGLUT puncta, those immunolabeled for VGLUT2 were the most abundant in the DR. In previous studies using conventional methods it was very difficult to draw conclusions regarding relative abundance of different groups of axons due to the issue of potential differences in antibody penetration through a thick section; however, the abundance of VGLUT2-immunolabeled puncta is consistent with previous subjective impressions (Commons et al., 2005). When we analyzed VGLUT puncta with the criteria for apposition with PSD-95, a substantial proportion of VGLUT puncta were eliminated from the analysis. However, in this analysis differences in abundance between VGLUT types became more pronounced, and again VGLUT2 predominated. It should be noted that one factor that may contribute to this finding is the potential for differences in PSD-95 content at synapses associated with each VGLUT. That is, VGLUT3-positive boutons have been reported to form both asymmetric and symmetric synapses, the latter of which may have subtle postsynaptic densities and possibly less PSD-95 (Gras et al., 2002). In contrast, VGLUT2-containing axons overwhelmingly form asymmetric synapses in the DR (Commons et al., 2005).

Glutamatergic innervation of 5-HT vs. non-5-HT neurons

A substantial proportion of the glutamatergic axons apposed to PSD-95 was not associated with 5-HT cells, and therefore likely reflects innervation of non-5-HT neurons in the DR. Previous studies have shown that VGLUT1- and VGLUT2-positive axons establish synapses with dendrites that lack TPOH immunolabeling (Commons et al., 2005). In addition, cortical projections have been shown to innervate and modulate non-5-HT and specifically GABAergic cells (Celada et al., 2001; Jankowski and Sesack, 2004). The fraction of VGLUT/PSD-95 pairs that were found in association to TPOH ranged from 23–32%, which is roughly consistent with previous estimates that only about one-third of the neurons in the DR contain 5-HT (Descarries et al., 1982).

The frequency with which glutamatergic axons associated with both PSD-95 and TPOH cells was not always proportionate to their overall abundance in the DR. That is, about 2-fold more VGLUT2 axons associated with PSD-95 than VGLUT1 or 3, but this relative proportion was not consistently reflected in association with 5-HT cells, although VGLUT2 axons retained overall predominance. There is evidence that glutamatergic innervation of 5-HT versus non-5-HT neurons in the DR is under differential regulatory mechanisms (Kirby et al., 2007). Taken together, these observations would suggest that 5-HT and non-5-HT neurons receive afferent innervation from different populations of glutamatergic axons. Furthermore, there were differences in the relative associations between different VGLUTs, PSD-95, and 5-HT cells in the dorsal and ventral parts of the DR. Previous retrograde labeling studies have shown that the ventromedial part of the DR receives innervation from a higher number of glutamate cells than the dorsomedial part (Lee et al., 2003). Thus, not only may 5-HT neurons receive different glutamatergic innervation than non-5-HT neurons, the organization of glutamatergic innervation of the DR may be subregionally specific.

In addition, our current results compare the distribution of VGLUT1- and VGLUT2-containing boutons to those with VGLUT3, which are known to be present within the DR (Gras et al., 2002; Herzog et al., 2004, Commons, 2009), but have not been comprehensively studied in comparison to the two other types of glutamatergic axons. While VGLUT3 is expressed in 5-HT neurons in the DR, previous analysis showed that most local VGLUT3-containing axons do not colocalize with markers of 5-HT, except in the caudal pole of the DR (Commons, 2009). Our current results indicate that a substantial proportion of VGLUT3-containing axons likely form asymmetric synapses onto 5-HT neurons in the DR. These VGLUT3 axons could primarily arise from a population of glutamatergic neurons in the DR that express the receptor for substance P, neurokinin 1 (Commons, 2009). This would be consistent with previous observations that substance P activates glutamatergic postsynaptic potentials in DR 5-HT neurons (Liu et al., 2002). That is, local VGLUT3-expressing cells activated by substance P have recurrent axon collaterals that provide excitatory drive to 5-HT neurons.

Glutamatergic neurotransmission in the DR and functional implications

This study shows that glutamate axons innervating the DR preferentially express VGLUT2. These likely arise from subcortical structures including the lateral habenula, hypothalamic nuclei, periaqueductal gray, and parabrachial nucleus (Kalén et al., 1985; Jolas and Aghajanian, 1997; Lee et al., 2003). VGLUT1- and VGLUT3-containing axons, whose sources include the prefrontal cortex and local glutamatergic neurons, respectively, are substantive secondary sources. Glutamatergic neurotransmission that regulates the activity of DR circuitry has been implicated in the progression of depressive illness (Paul and Skolnick, 2003). Moreover, in animal models glutamate receptor antagonists have shown to have antidepressant-like activity (Trullas and Skolnick, 1990; Maj et al., 1992; Papp and Moryl, 1996; Yilmaz et al., 2002). However, how specific circuits regulated by

glutamatergic synapses within the DR are topographically organized and selectively participate in emotional processing remains to be determined. Overall, our study indicates that array tomography represents a powerful approach to explore the fine molecular architecture of circuits in a well-preserved neuroanatomical context to understand circuit alterations that may be associated with psycopathological states.

Acknowledgments

Grant sponsor: National Institutes of Health; Grant number: DA021801.

LITERATURE CITED

Abbas AI, Yadav PN, Yao WD, Arbuckle MI, Grant SG, Caron MG, Roth BL. PSD-95 is essential for hallucinogen and atypical antipsychotic drug actions at serotonin receptors. J Neurosci. 2009; 29:7124–7136. [PubMed: 19494135]

Arango V, Underwood MD, Mann JJ. Serotonin brain circuits involved in major depression and suicide. Prog Brain Res. 2002; 136:443–453. [PubMed: 12143401]

Bellocchio EE, Reimer RJ, Fremeau RT Jr, Edwards RH. Uptake of glutamate into synaptic vesicles by an inorganic phosphate transporter. Science. 2000; 289:957–960. [PubMed: 10938000]

Bolte S, Cordelières FP. A guided tour into subcellular colocalization analysis in light microscopy. J Microsc. 2006; 224:213–232. [PubMed: 17210054]

Celada P, Puig MV, Casanovas JM, Guillazo G, Artigas F. Control of dorsal raphe serotonergic neurons by the medial prefrontal cortex: involvement of serotonin-1A, GABA(A), and glutamate receptors. J Neurosci. 2001; 21:9917–9929. [PubMed: 11739599]

Cheng D, Hoogenraad CC, Rush J, Ramm E, Schlager MA, Duong DM, Xu P, Wijayawardana SR, Hanfelt J, Nakagawa T, Sheng M, Peng J. Relative and absolute quantification of postsynaptic density proteome isolated from rat forebrain and cerebellum. Mol Cell Proteomics. 2006; 5:1158–1170. [PubMed: 16507876]

Commons KG. Locally collateralizing glutamate neurons in the dorsal raphe nucleus responsive to substance P contain vesicular glutamate transporter 3 (VGLUT3). J Chem Neuroanat. 2009; 38:273–281. [PubMed: 19467322]

Commons KG, Serock MR. Coincidence of neurokinin 1 receptor with the vesicular glutamate transporter 3 (VGLUT3) in the rat forebrain. Neurosci Lett. 2009; 464:188–192. [PubMed: 19699779]

Commons KG, Beck SG, Bey VW. Two populations of glutamatergic axons in the rat dorsal raphe nucleus defined by the vesicular glutamate transporters 1 and 2. Eur J Neurosci. 2005; 21:1577–1586. [PubMed: 15845085]

Datwani A, McConnell MJ, Kanold PO, Micheva KD, Busse B, Shamloo M, Smith SJ, Shatz CJ. Classical MHCI molecules regulate retinogeniculate refinement and limit ocular dominance plasticity. Neuron. 2009; 64:463–470. [PubMed: 19945389]

Descarries L, Watkins KC, Garcia S, Beaudet A. The serotonin neurons in nucleus raphe dorsalis of adult rat: a light and electron microscope radioautographic study. J Comp Neurol. 1982; 207:239–254. [PubMed: 7107985]

Freitas RL, Bassi GS, de Oliveira AM, Coimbra NC. Serotonergic neurotransmission in the dorsal raphe nucleus recruits in situ 5-HT(2A/2C) receptors to modulate the post-ictal antinociception. Exp Neurol. 2008; 213:410–418. [PubMed: 18671968]

Fremeau RT Jr, Troyer MD, Pahner I, Nygaard GO, Tran CH, Reimer RJ, Bellocchio EE, Fortin D, Storm-Mathisen J, Edwards RH. The expression of vesicular glutamate transporters defines two classes of excitatory synapse. Neuron. 2001; 31:247–260. [PubMed: 11502256]

Fremeau RT Jr, Burman J, Qureshi T, Tran CH, Proctor J, Johnson J, Zhang H, Sulzer D, Copenhagen DR, Storm-Mathisen J, Reimer RJ, Chaudhry FA, Edwards RH. The identification of vesicular glutamate transporter 3 suggests novel modes of signaling by glutamate. Proc Natl Acad Sci U S A. 2002; 99:14488–14493. [PubMed: 12388773]

Fu W, Le Maître E, Fabre V, Bernard JF, David Xu ZQ, Ho¨kfelt T. Chemical neuroanatomy of the dorsal raphe nucleus and adjacent structures of the mouse brain. J Comp Neurol. 2010; 518:3464–3494. [PubMed: 20589909]

Gabellec MM, Panzanelli P, Sassoè-Pognetto M, Lledo PM. Synapse-specific localization of vesicular glutamate transporters in the rat olfactory bulb. Eur J Neurosci. 2007; 25:1373–1383. [PubMed: 17425564]

Gras C, Herzog E, Bellenchi GC, Bernard V, Ravassard P, Pohl M, Gasnier B, Giros B, El Mestikawy S. A third vesicular glutamate transporter expressed by cholinergic and serotoninergic neurons. J Neurosci. 2002; 22:5442–5451. [PubMed: 12097496]

Han K, Kim E. Synaptic adhesion molecules and PSD-95. Prog Neurobiol. 2008; 84:263–283. [PubMed: 18206289]

Herzog E, Bellenchi GC, Gras C, Bernard V, Ravassard P, Bedet C, Gasnier B, Giros B, El Mestikawy S. The existence of a second vesicular glutamate transporter specifies subpopulations of glutamatergic neurons. J Neurosci. 2001; 21:RC181. [PubMed: 11698619]

Herzog E, Gilchrist J, Gras C, Muzerelle A, Ravassard P, Giros B, Gaspar P, El Mestikawy S. Localization of VGLUT3, the vesicular glutamate transporter type 3, in the rat brain. Neuroscience. 2004; 123:983–1002. [PubMed: 14751290]

Hioki H, Fujiyama F, Nakamura K, Wu SX, Matsuda W, Kaneko T. Chemically specific circuit composed of vesicular glutamate transporter 3- and preprotachykinin B-producing interneurons in the rat neocortex. Cereb Cortex. 2004; 14:1266–1275. [PubMed: 15142960]

Hioki H, Nakamura H, Ma YF, Konno M, Hayakawa T, Nakamura KC, Fujiyama F, Kaneko T. Vesicular glutamate transporter 3-expressing nonserotonergic projection neurons constitute a subregion in the rat midbrain raphe nuclei. J Comp Neurol. 2010; 518:668–686. [PubMed: 20034056]

Jacobs BL, Azmitia EC. Structure and function of the brain serotonin system. Physiol Rev. 1992; 72:165–229. [PubMed: 1731370]

Jankowski MP, Sesack SR. Prefrontal cortical projections to the rat dorsal raphe nucleus: ultrastructural features and associations with serotonin and gamma-aminobutyric acid neurons. J Comp Neurol. 2004; 468:518–529. [PubMed: 14689484]

Jolas T, Aghajanian GK. Opioids suppress spontaneous and NMDA-induced inhibitory postsynaptic currents in the dorsal raphe nucleus of the rat in vitro. Brain Res. 1997; 755:229–245. [PubMed: 9175891]

Kalén P, Karlson M, Wiklund L. Possible excitatory amino acid afferents to nucleus raphe dorsalis of the rat investigated with retrograde wheat germ agglutinin and D-[3H]aspartate tracing. Brain Res. 1985; 360:285–297. [PubMed: 2866825]

Kaneko T, Fujiyama F. Complementary distribution of vesicular glutamate transporters in the central nervous system. Neurosci Res. 2002; 42:243–250. [PubMed: 11985876]

Kaneko T, Fujiyama F, Hioki H. Immunohistochemical localization of candidates for vesicular glutamate transporters in the rat brain. J Comp Neurol. 2002; 444:39–62. [PubMed: 11835181]

Keith D, El-Husseini A. Excitation control: balancing PSD-95 function at the synapse. Front Mol Neurosci. 2008; 1:4. [PubMed: 18946537]

Kirby LG, Pan YZ, Freeman-Daniels E, Rani S, Nunan JD, Akanwa A, Beck SG. Cellular effects of swim stress in the dorsal raphe nucleus. Psychoneuroendocrinology. 2007; 32:712–723. [PubMed: 17602840]

Koffie RM, Meyer-Luehmann M, Hashimoto T, Adams KW, Mielke ML, Garcia-Alloza M, Micheva KD, Smith SJ, Kim ML, Lee VM, Hyman BT, Spires-Jones TL. Oligomeric amyloid beta associates with postsynaptic densities and correlates with excitatory synapse loss near senile plaques. Proc Natl Acad Sci U S A. 2009; 106:4012–4017. [PubMed: 19228947]

Lee HS, Kim MA, Valentino RJ, Waterhouse BD. Glutamatergic afferent projections to the dorsal raphe nucleus of the rat. Brain Res. 2003; 963:57–71. [PubMed: 12560111]

Liu R, Ding Y, Aghajanian GK. Neurokinins activate local glutamatergic inputs to serotonergic neurons of the dorsal raphe nucleus. Neuropsychopharmacology. 2002; 27:329–340. [PubMed: 12225691]

Maj J, Rogóz Z, Skuza G, Sowińska H. Effects of MK-801 and antidepressant drugs in the forced swimming test in rats. Eur Neuropsychopharmacol. 1992; 2:37–41. [PubMed: 1638172]

Melone M, Burette A, Weinberg RJ. Light microscopic identification and immunocytochemical characterization of glutamatergic synapses in brain sections. J Comp Neurol. 2005; 492:495–509. [PubMed: 16228991]

Micheva KD, Smith SJ. Array tomography: a new tool for imaging the molecular architecture and ultrastructure of neural circuits. Neuron. 2007; 55:25–36. [PubMed: 17610815]

Micheva KD, Busse B, Weiler NC, O'Rourke N, Smith SJ. Single-synapse analysis of a diverse synapse population: proteomic imaging methods and markers. Neuron. 2010a; 68:639–653. [PubMed: 21092855]

Micheva, KD.; O'Rourke, N.; Busse, B.; Smith, SJ. Array tomography: high-resolution 3D immunofluorescence. In: Yuste, R., editor. Optical imaging techniques: a laboratory manual. Cold Spring Harbor, NY: Cold Spring Harbor Laboratory Press; 2010b. p. 697-719.

Molliver ME. Serotonergic neuronal systems: what their anatomic organization tells us about function. J Clin Psychopharmacol. 1987; 7:3S–23S. [PubMed: 3323265]

Papp M, Moryl E. Antidepressant-like effects of 1-aminocyclopropanecarboxylic acid and D-cycloserine in an animal model of depression. Eur J Pharmacol. 1996; 316:145–151. [PubMed: 8982680]

Paul IA, Skolnick P. Glutamate and depression: clinical and preclinical studies. Ann N Y Acad Sci. 2003; 1003:250–272. [PubMed: 14684451]

Paxinos, G.; Franklin, KBJ. The mouse brain in stereotaxic coordinates. San Diego: Academic Press; 2001.

Peng J, Kim MJ, Cheng D, Duong DM, Gygi SP, Sheng M. Semiquantitative proteomic analysis of rat forebrain postsynaptic density fractions by mass spectrometry. J Biol Chem. 2004; 279:21003–21011. [PubMed: 15020595]

Schäfer MK, Varoqui H, Defamie N, Weihe E, Erickson JD. Molecular cloning and functional identification of mouse vesicular glutamate transporter 3 and its expression in subsets of novel excitatory neurons. J Biol Chem. 2002; 277:50734–50748. [PubMed: 12384506]

Shutoh F, Ina A, Yoshida S, Konno J, Hisano S. Two distinct subtypes of serotonergic fibers classified by co-expression with vesicular glutamate transporter 3 in rat forebrain. Neurosci Lett. 2008; 432:132–136. [PubMed: 18222609]

Steinbusch HW. Distribution of serotonin-immunoreactivity in the central nervous system of the rat-cell bodies and terminals. Neuroscience. 1981; 6:557–618. [PubMed: 7017455]

Steinbusch, W. Serotonin-immunoreactive neurons and their projections in the CNS. In: Bjorklund, A.; Hokfelt, T., editors. Handbook of chemical neuroanatomy. New York: Elsevier; 1984. p. 68-125.

Stockmeier CA. Neurobiology of serotonin in depression and suicide. Ann N Y Acad Sci. 1997; 836:220–232. [PubMed: 9616801]

Takahashi A, Shimamoto A, Boyson CO, DeBold JF, Miczek KA. GABA(B) receptor modulation of serotonin neurons in the dorsal raphé nucleus and escalation of aggression in mice. J Neurosci. 2010; 30:11771–11780. [PubMed: 20810897]

Theévenaz P, Ruttimann UE, Unser M. A pyramid approach to subpixel registration based on intensity. IEEE Trans Image Process. 1998; 7:27–41. [PubMed: 18267377]

Trullas R, Skolnick P. Functional antagonists at the NMDA receptor complex exhibit antidepressant actions. Eur J Pharmacol. 1990; 185:1–10. [PubMed: 2171955]

van Steensel B, van Binnendijk E, Hornsby C, van der Voort H, Krozowski Z, de Kloet E, van Driel R. Partial colocalization of glucocorticoid and mineralocorticoid receptors in discrete compartments in nuclei of rat hippocampus neurons. J Cell Sci. 1996; 109:787–792. [PubMed: 8718670]

VanderHorst VG, Ulfhake B. The organization of the brainstem and spinal cord of the mouse: relationships between monoaminergic, cholinergic, and spinal projection systems. J Chem Neuroanat. 2006; 31:2–36. [PubMed: 16183250]

Varoqui H, Schäfer MK, Zhu H, Weihe E, Erickson JD. Identification of the differentiation-associated Na+/PI transporter as a novel vesicular glutamate transporter expressed in a distinct set of glutamatergic synapses. J Neurosci. 2002; 22:142–155. [PubMed: 11756497]

Yilmaz A, Schulz D, Aksoy A, Canbeyli R. Prolonged effect of an anesthetic dose of ketamine on behavioral despair. Pharmacol Biochem Behav. 2002; 71:341–344. [PubMed: 11812542]

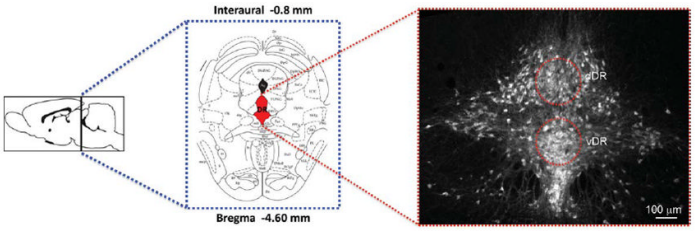

Figure 1.

Sampling subregions in the mouse DR. Schematic representations of the brain level and coronal section containing the area of interest, the mid-DR, adapted from the mouse brain atlas (Paxinos and Franklin, 2001) (left). Photomicrographs illustrating the distribution of serotonergic neurons, identified by TPOH immunolabeling at the mid-DR divided into dorsal (d) and ventral (v) midline subregions (right). Red areas represent areas of the DR that were sampled for analysis using array tomography. [Color figure can be viewed in the online issue, which is available at wileyonlinelibrary.com.]

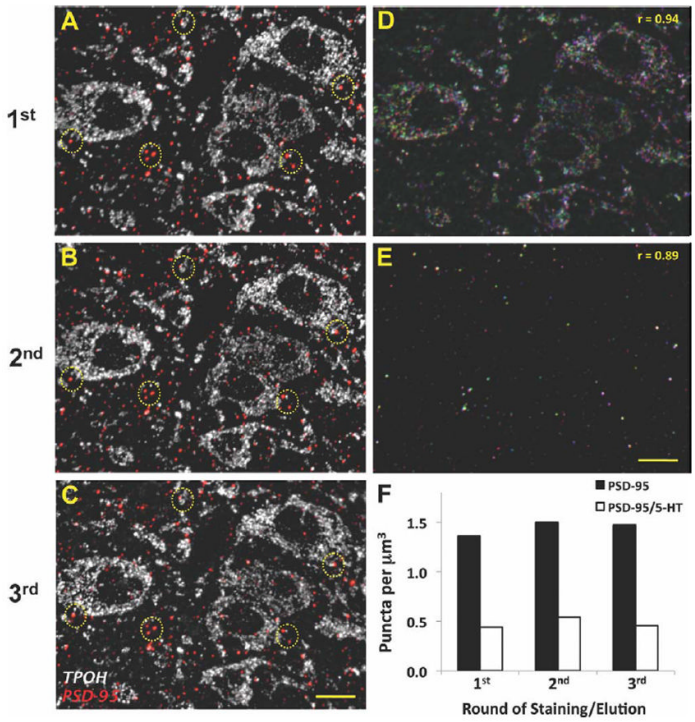

Figure 2.

Preservation of antigenicity for PSD-95 and TPOH after multiple rounds of antibodies staining/elution in array tomography. **A–C**: The same 70-nm ultrathin section labeled against PSD-95 (red) and TPOH (white) in three consecutive rounds of staining/elution showing highly similar patterns of labeling. Examples of the PSD-95 immunolabeling repeated in each round are shown within yellow circles. Controls where primary antisera were omitted confirmed immunolabeling was completely removed by elution procedure. **D,E**: Merged images from the same 70-nm section labeled for TPOH (upper panel) and PSD-95 (lower panel) in three consecutive rounds of staining/elution. The first round of staining is pseudocolored in blue, the second in red, and the third one in green. Overlapping pixels are shown in white. **F**: Quantitative analysis of PSD-95 puncta density either associated or not with TPOH-positive areas for the same stack of images after three rounds of antibodies staining/elution. Scale bars = 10 µm. [Color figure can be viewed in the online issue, which is available at wileyonlinelibrary.com.]

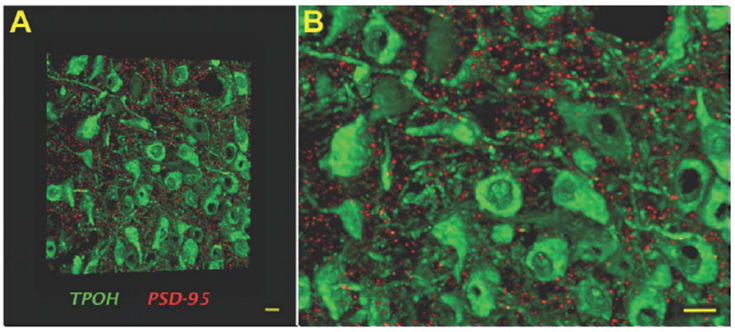

Figure 3.

Volumetric image of labeling for TPOH and PSD-95 in the mouse DR, illustrating the high-resolution achieved in array tomography. **A**: A volume rendering of 30 ultrathin (70 nm) serial sections showing a high density of TPOH-positive cells (green) abundantly surrounded by discrete PSD-95 puncta (red). **B**: Zoomed-in view of (A) indicating the absence of out of focus light resulting in high-resolution images amenable to quantitative analysis. Scale bars = 10 μm. [Color figure can be viewed in the online issue, which is available at wileyonlinelibrary.com.]

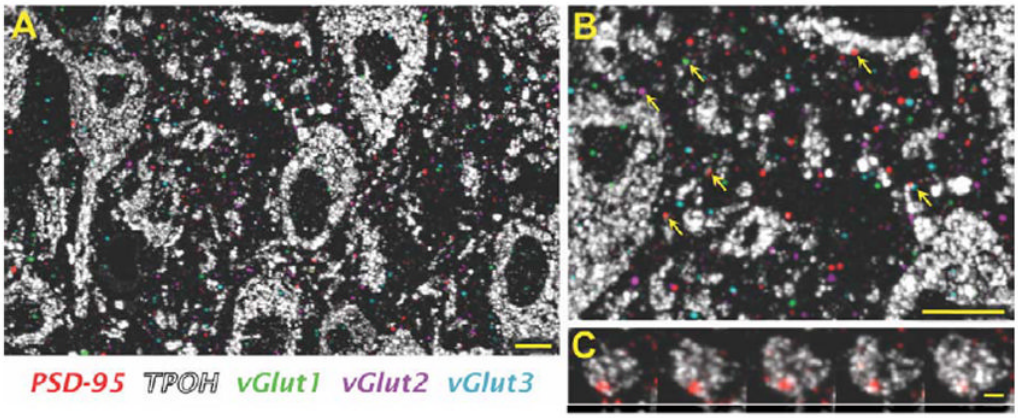

Figure 4.

All three types of VGLUT and PSD-95 are widely distributed in the mouse DR. **A**: An image of a single 70-nm section showing a high density of TPOH-positive cells (white) within the DR, densely surrounded by PSD-95 (red), VGLUT1 (green), VGLUT2 (magenta), and VGLUT3 (light blue). Notice that because this is a single 70-nm section image several VGLUT puncta that apparently lack a PSD-95 postsynaptic partner may have it in an adjacent section. **B**: Zoomed-in view of (A), indicating possible associations of all three types of VGLUT and PSD-95 with TPOH-positive cells (arrows). **C**: Serial section images through an individual PSD-95 punctum associated with a 5-HT cell. Scale bars = 10 μm in A,B; 2 μm in C. [Color figure can be viewed in the online issue, which is available at wileyonlinelibrary.com.]

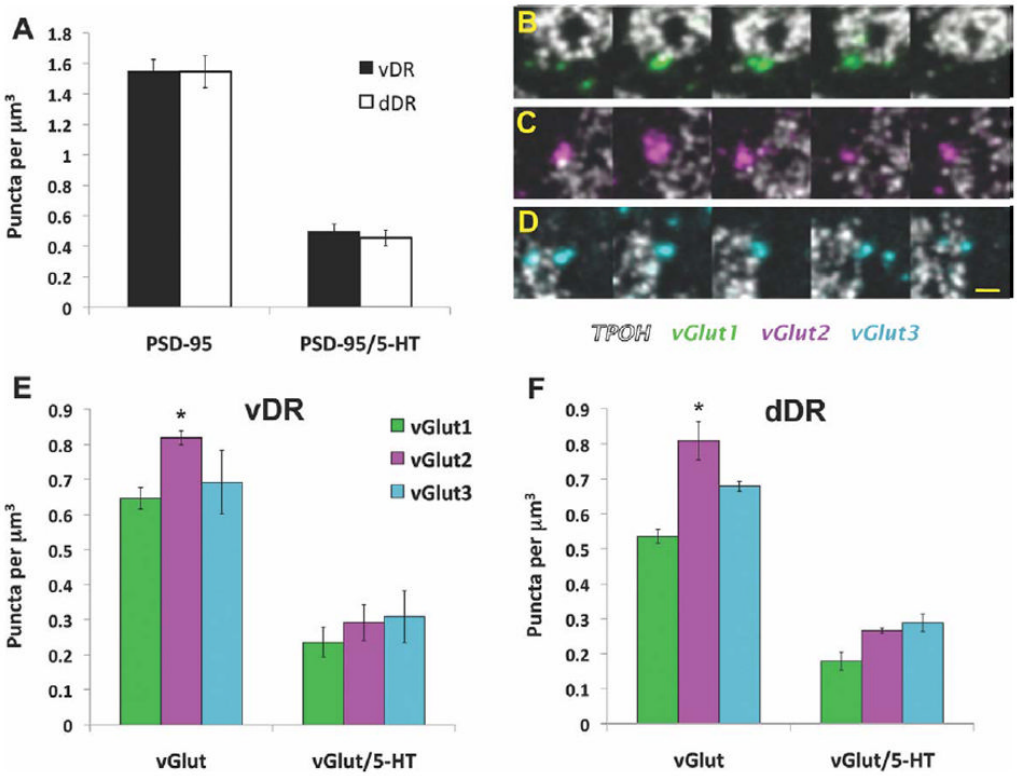

Figure 5.

Quantitative analysis of PSD-95 and VGLUT puncta in the mouse DR. **A**: Density of PSD-95 puncta, and their association with 5-HT cells in the ventral (vDR) and dorsal (dDR) parts of the DR. **B–D**: Serial section images through individual VGLUT1 (green), VGLUT2 (magenta), and VGLUT3 (light blue) puncta, respectively, in association with 5-HT cells (white). **E,F**: Density of VGLUT puncta and their associations with 5-HT cells in the vDR and dDR, respectively. *$P < 0.002$ vs. VGLUT1. Scale bar = 2 µm in D (applies to B,C). [Color figure can be viewed in the online issue, which is available at wileyonlinelibrary.com.]

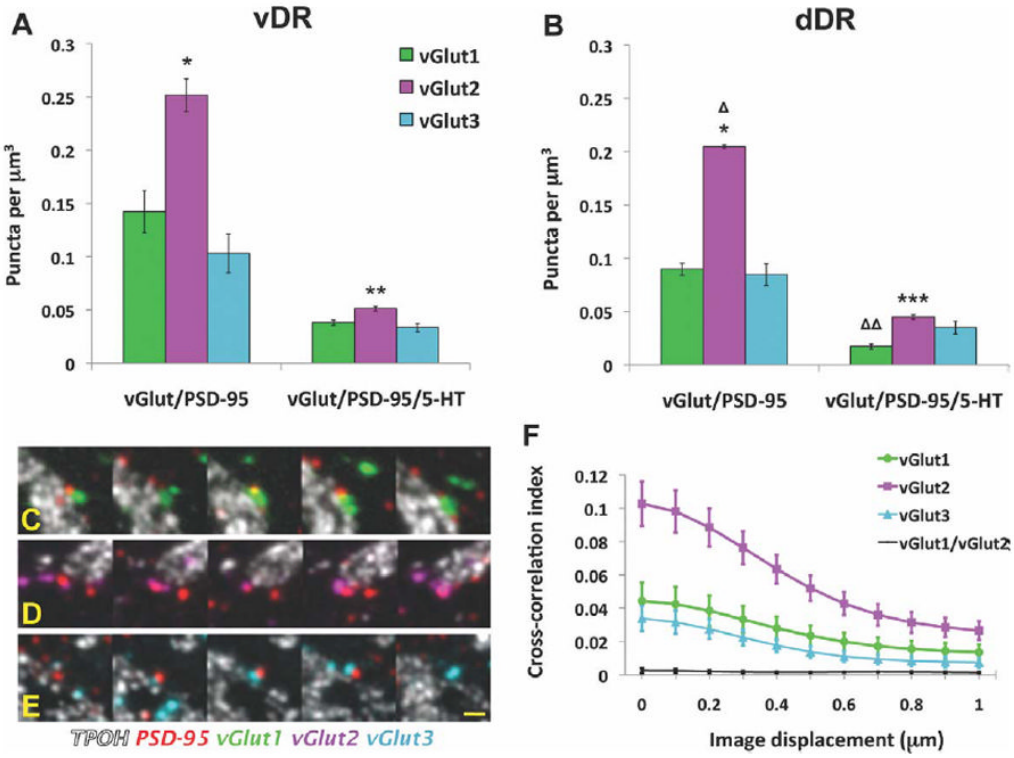

Figure 6.

Quantitative analysis of VGLUT/PSD-95 puncta appositions in the mouse DR. **A,B**: Density of VGLUT/PSD-95 puncta appositions, and their association with 5-HT cells in the ventral (vDR) and dorsal (dDR) parts of the DR, respectively. **C–E**: Serial section images of appositions containing VGLUT1 (green), VGLUT2 (magenta), or VGLUT3 (light blue), respectively, in association with 5-HT cells (white). **F**: Cross-correlation analysis of pixels for PSD-95 and VGLUT1 (green), VGLUT2 (magenta), or VGLUT3 (light blue) puncta in the DR. The control analysis of the poorly colocalized VGLUT1 and VGLUT2 puncta is also shown (black). $^{*}P < 10^{-4}$ vs. either VGLUT1 or VGLUT3. $^{**}P < 0.02$ vs. VGLUT3. $^{\Delta}P < 0.004$ for dDR VGLUT/PSD-95 vs. vDR. $^{***}P < 0.05$ vs. either VGLUT1 or VGLUT3. $^{\Delta\Delta}P < 0.003$ for dDR VGLUT1/PSD-95/5-HT vs. vDR. Scale bar = 2 µm in E (applies to C,D). [Color figure can be viewed in the online issue, which is available at wileyonlinelibrary.com.]

TABLE 1

Antisera Used for Array Tomography

Antigen	Immunogen	Manufacturer	Dilution
VGLUT1	Synthetic peptide from rat VGLUT1 (aa 542-560)	Millipore (Billerica, MA), guinea pig polyclonal, AB5905	1:1,000
VGLUT2	Recombinant GST-tagged C-terminal peptide of rat VGLUT2 (VQESAQDAYSYKDRDDYS)	Millipore (Billerica, MA), guinea pig polyclonal, AB2251	1:1,000
VGLUT3	Synthetic peptide from rat VGLUT3 (aa 569-588)	Millipore (Billerica, MA), guinea pig polyclonal, AB5421	1:1,000
Tryptophan hydroxylase	Recombinant rabbit tryptophan hydroxylase, isolated as inclusion bodies from E. coli	Millipore (Billerica, MA), sheep polyclonal, AB1541	1:200
PSD-95	Synthetic peptide (KLH-coupled) from human PSD-95 (aa 42-63)	Cell Signaling Technology (Danvers, MA), rabbit monoclonal, D27E11 XP #3450	1:200
Synapsin I	Synapsin I (mixture of Ia and Ib) purified from bovine brain	Millipore (Billerica, MA), rabbit polyclonal, AB1543	1:100